

## Effects of substitutional Ga on the phonons of $\delta$ -phase Pu based on density functional theory calculations

Sven P. Rudin <sup>\*</sup>*Los Alamos National Laboratory, Los Alamos, New Mexico 87545, USA*

(Received 25 February 2022; revised 27 April 2022; accepted 3 May 2022; published 17 May 2022)

The delta phase of Pu is stabilized by Ga doping, but the mechanism of this stabilization remains an open question. Density functional theory calculations focused on how Ga doping affects the phonons sheds some light on the phonons' contribution to the stabilization. The calculated phonon modes of Ga-doped delta phase Pu fall into two distinct types: localized, high frequency Ga-dominated phonon modes, and Pu-dominated modes at lower frequencies. Increasing the Ga concentration has an effect on the Pu-dominated phonon modes opposite to that of compression: higher-frequency modes soften, and lower-frequency modes stiffen. The latter provides an indication that the stabilization mechanism is not due to a thermodynamic contribution from the phonons. Furthermore, the stiffened phonon modes include candidate modes that describe possible pathways into low-temperature phases, suggesting that doping with Ga could impede such pathways.

DOI: [10.1103/PhysRevB.105.184107](https://doi.org/10.1103/PhysRevB.105.184107)

### I. INTRODUCTION

Phonons contribute critically to controlling the thermal properties of crystalline materials. As phonons are the normal modes of vibration of the crystal lattice, the structure of the lattice determines how the forces between the atoms translate into phonon frequencies and eigenmodes. Accordingly, lattice imperfections change the phonons and hence the material's thermal properties. Imperfections such as stacking faults and point defects represent flaws in the periodicity of the material's crystal structure, but their presence can be desirable or undesirable depending on a material's application [1]. Many desirable thermal properties are achieved by introducing point defects by way of targeted doping. Among the desired properties, and of particular interest here, is the stabilization of crystal structure phases into wider temperature ranges.

Doping Pu with small amounts of Ga stabilizes the delta phase to lower temperatures [2]. In its pure form,  $\delta$ -Pu is stable in the 315–450 °C range, doping with a few atomic % Ga extends the range to well below room temperature.

The mechanism of this stabilization remains unclear. This lack of clarity is reflected in contradictory phase diagrams [3,4] constructed to reflect thermodynamic equilibrium. In one diagram, Ga-doped  $\delta$ -Pu remains stable to temperatures below 0 °C, in the other diagram Ga-doped  $\delta$ -Pu decomposes to a mixture of  $\alpha$ -Pu and Pu<sub>3</sub>Ga. Self-irradiation in  $\delta$ -Pu continuously introduces additional lattice imperfections, making a purely experimental resolution of the stabilization mechanism a challenge. Because the changing population of lattice imperfections changes thermal properties, understanding the stabilization mechanism is crucial to controlling the thermal properties of aging Ga-doped  $\delta$  Pu.

The challenge motivates calculations that examine possible stabilization mechanisms. Among the mechanisms proposed based on density functional theory (DFT) calculations are a stabilizing effect of Ga on a disordered magnetic state, thereby allowing the  $\delta$ -Pu phase to be preserved at lower temperatures [5] and a reduction in the enthalpy for transformation from  $\delta$  to  $\alpha$  with increased Ga concentration [6]. Calculated bond strengths between a Ga atom and its Pu neighbors in  $\delta$ -Pu show that the Ga-Pu bonds are more uniform and symmetric than the Pu-Pu bonds, suggesting that changes to the bonding stabilize the delta phase [7,8], driven by hybridization of the Pu 6*d* and Ga 4*p* states [9,10]. Further calculations show a softening of the elastic moduli with increased Ga concentration [11], indicating a softening of the lower-frequency phonons, whose increased contribution to the entropy thereby supports a phonon-driven thermodynamic mechanism for stabilization.

Examining the phonons is appropriate because structural phase transformations rarely occur without involving the phonons. They influence the thermodynamics by affecting the free energy and, in some systems, describe (part of) the pathway the atoms take between phases. Indeed, Wong *et al.* [12] observed a candidate phonon mode that shows anomalous behavior in the measured phonon dispersion curves of Ga-stabilized  $\delta$  Pu: a soft transverse mode at the Brillouin zone boundary,  $T[111]$ , that suggests neighboring (111) planes could be easily sheared against each other, thereby pushing  $\delta$ -Pu toward  $\alpha$ -Pu. The expected phonon softening, a lowering of the mode's frequency, is, however, not observed in Ga-stabilized  $\delta$  Pu: the mode shows little to no temperature dependence between 200 K and 307 K [13], in agreement with its calculated behavior in undoped  $\delta$ -Pu [14]. Nonetheless, the anomalous behavior also appears for shorter wave vectors of the  $T[\xi\xi\xi]$  branch, which includes a candidate phonon mode that, based on symmetry arguments, initiates a possible pathway into the low-temperature phase [15,16].

\*srudin@lanl.gov

This contribution addresses the Ga stabilization of  $\delta$ -Pu by calculating how Ga substitution affects the phonons of  $\delta$ -Pu. The Ga atoms are assumed to be substitutional, as indicated by experiment and supported by calculations [17,18]. Section II provides the details of the calculations, including a method to trace how phonon modes of the undoped structure map into the phonon modes of the Ga-doped structure. Results presented in Sec. III report two effects of a single substitutional Ga in  $\delta$ -Pu: it creates a local, Ga-dominated high-frequency mode and it stiffens the low-frequency modes (Sec. III B). These two effects are subsequently shown to persist with increasing Ga concentration (Sec. III C). The calculations for these results are performed at the experimental lattice constant,  $a_0 = 4.64 \text{ \AA}$ . Further results show that, while compression of  $\delta$ -Pu *softens* some of the low-frequency phonon modes, the Ga-induced stiffening of the low-frequency modes exceeds the softening. Taken together, these results suggest Ga doping could impede the proposed pathways from the delta phase into the alpha phase, as discussed in Sec. IV.

## II. METHODS

The present paper considers only the harmonic phonons, calculated with density functional theory as implemented in the VASP package [19,20]. The electronic states are treated with the projector augmented wave method [21] in the generalized gradient approximation of Perdew *et al.* [22] with first-order Methfessel-Paxton smearing (width 27 meV) [23] and a cutoff energy for the plane-wave basis set of 500 eV. The k-point meshes are chosen for each simulation cell such that their density is at least 40 per  $\text{\AA}^{-3}$ . Increasing this density to at least 60 per  $\text{\AA}^{-3}$  for the 72-atom system with one Ga (a change of k-point mesh from  $3 \times 3 \times 4$  to  $4 \times 4 \times 6$ ) shows good convergence: phonon frequencies change by less than 3%, and phonon mode tracing (defined below) shows no significant changes to the corresponding modes' eigenvector (Fig. 1 in the SM [24]). The phonon moments, which serve as measures of the phonon density of states relevant for thermodynamics, change by 0.3%. They are defined on pp. 149–152 of Ref. [25],

$$\ln(\omega_0) = \langle \ln(\omega) \rangle, \quad \omega_1 = \frac{4}{3} \langle \omega \rangle, \quad \text{and} \quad \omega_2 = \sqrt{\frac{5}{3} \langle \omega^2 \rangle}, \quad (1)$$

where the average  $\langle \dots \rangle$  is over all phonon frequencies (omitting the three translational modes).

The convergence criteria are  $10^{-8}$  eV for the electronic self-consistency loop and  $10^{-7}$  eV for the ionic relaxation. Following Ref. [6], spin-orbit coupling and orbital polarization are neglected in the interest of making the large number of calculations on large system sizes, required for evaluation of the phonons, computationally feasible. The importance of spin-orbit coupling and orbital polarization, however, should not be neglected.

The calculations employ the experimental equilibrium volume of  $\delta$ -Pu, with a few exceptions. The use of a single volume serves to focus on how the Ga substitutions affect the phonon modes directly, without adding effects due to changing volume—these are considered separately at the end. The use of the experimental rather than the theoretical volume is motivated by the experience that, while DFT cold curves

(zero-temperature energy versus volume curves) are known to be in error for many materials, phonon frequencies calculated at the experimental geometric parameters tend to be in good agreement with measured frequencies. This experience is reflected, e.g., in the construction of equations of state, where DFT cold curves are shifted to agree with experimental data while DFT phonon data are used at the volume for which they are calculated [26,27].

The effects of strongly correlated  $5f$  electrons are approximated by allowing spin polarization [28]. Applied to Pu, spin-polarized DFT calculations successfully describe many of the material's remarkable and unusual facets accurately [29–32]. This approach has its critics since magnetic moments are not observed [33]. Alternatively, Pu exhibits a fluctuating magnetic structure [34] in which case the choice of ordered, or disordered [35], magnetic structures can be viewed as static snapshots of the fluctuations [36]. From a practical point of view of calculating structural parameters and forces in large systems, however, spin-polarized DFT calculations appear as a reasonable approximation. Furthermore, doping  $\delta$ -Pu with Ga stabilizes the antiferromagnetic (AFM) structure in DFT calculations [37] and experimental measurements indicate a stable AFM structure for  $\text{Pu}_{0.92}\text{Ga}_{0.08}$  at low temperatures [38]. In addition to being the lowest-energy magnetic structure in DFT calculations, the AFM structure represents multiple degenerate magnetic structures when all the commensurate phonons are considered together. More advanced methods such as DMFT are not feasible for these systems and their phonons, as their application is currently too computationally expensive. Another alternative method, DFT + U results in unstable modes [39].

The zero-temperature phonons are calculated with the small-displacement method [40–42]. Inequivalent atoms in the computational cells are displaced by  $0.015 \text{ \AA}$  in all symmetry-inequivalent Cartesian directions and the forces calculated with DFT serve to construct the Hessian matrix. For a system with  $N$  atoms at equilibrium positions  $\mathbf{R}_i$ , diagonalizing the Hessian delivers the  $3N$  phonon modes  $n$ , each described by an eigenvector  $\epsilon_n(\mathbf{R}_i)$  and a frequency  $\omega_n$ . The eigenvectors are normalized so  $\sum_i \epsilon_n(\mathbf{R}_i) = 1$ . This allows the identification of  $(\epsilon_n(\mathbf{R}_i))^2$  as the weight of phonon mode  $n$  on atom  $i$ .

To investigate how changes to a system affect the phonon modes, the eigenvectors of the phonon modes with and without the Ga doping are projected onto each other. In the case of substitutional doping of  $\delta$ -Pu with Ga, this amounts to a bilinear projection from the Ga-doped system to the undoped system and individual Ga atom(s). The projection relies on a one-to-one mapping of atoms, in which (i) the Pu atoms in the doped system  $\beta$  map to the corresponding Pu atoms in the undoped system (system  $\alpha 1$ ) and (ii) the Ga atoms in the doped system  $\beta$  map to independent Ga atoms (system  $\alpha 2$ ). The phonons of independent Ga atoms are the three translational modes with zero frequency.

The projection provides information about changes to the phonon modes that goes beyond changes to the phonon density of states (DOS). Changes to the DOS account for changes to the thermodynamics but understanding changes to individual modes, in particular, the  $T[111]$  mode, requires more detail. While phonon dispersions show detail, once

substitutional atoms are introduced these need to be either calculated for supercells of the already large doped systems' unit cells, or the phonon dispersion needs to be approximated onto those of the undoped system by assuming the eigenmodes do not change. While the latter can, in principle, be compared to experimental phonon dispersions, it fails to deliver the details sought here. The bilinear projection from the doped system  $\beta$  into the undoped system  $\alpha 1$  and the dopant system  $\alpha 2$  allows the definition of the weight  $w(n(\beta), m(\alpha k))$  of a phonon mode  $n(\beta)$  of the doped system  $\beta$  on a phonon mode  $m(\alpha k)$  of the undoped or dopant system  $\alpha k$ :

$$w(n(\beta), m(\alpha k)) = \left( \sum_{i \in \alpha k} \epsilon_{n(\beta)}(\mathbf{R}_i) \epsilon_{m(\alpha k)}(\mathbf{R}_i) \right)^2. \quad (2)$$

These weights trace (hence the phonon tracing terminology) how individual phonon modes in the undoped or dopant systems relate to individual phonon modes in the doped system.

### III. RESULTS

#### A. Comparisons with experiment and previous calculations

Before calculating the effects of Ga doping, the quality of the methods used here is put into perspective. Figure 1 compares the calculated phonon dispersion of undoped  $\delta$ -Pu with results from experiments [12] and other calculations [36,43]. The symmetry breaking due to the AFM structure is evident in differences between the [00 $x$ ] and the [ $x$ 00] directions and in the lifting of some degeneracies. Aside from the symmetry breaking, the agreement with experiment overall is on par with that of other calculations.

The experimental data compared to above is from  $\delta$ -Pu that was stabilized at room temperature by doping with 2 at. % Ga [12]. Figure 2(a) compares the phonon DOS derived from those data with the results from a calculation with 1.4 at. % Ga. Similarly, Fig. 2(b) compares the phonon DOS directly

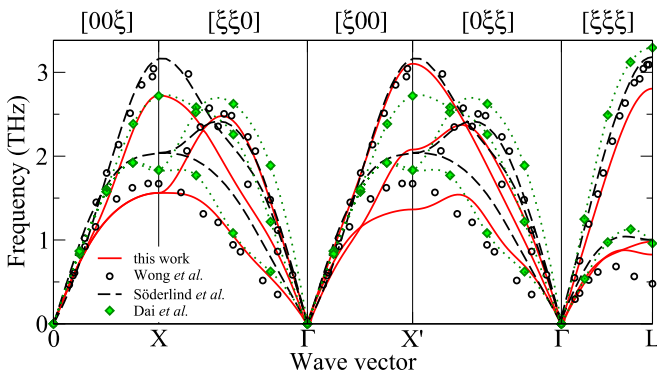


FIG. 1. Comparison of the  $\delta$ -Pu phonon dispersion with experiment and other calculations. The dispersion in this paper is calculated with the AFM structure in a computational cell with 96 atoms at  $a_0 = 4.64 \text{ \AA}$ . Unlike experiments (Wong *et al.* [12]) and other calculations (Söderlind *et al.* [36], Dai *et al.* [43]), the AFM structure breaks the cubic symmetry by singling out the [00 $x$ ] direction for the wave vector of the magnetic structure: consequently, the results are shown along more high symmetry directions than required for the fcc structure. The experimental data is from measurements on a  $\delta$ -Pu sample with 2 at. % Ga.

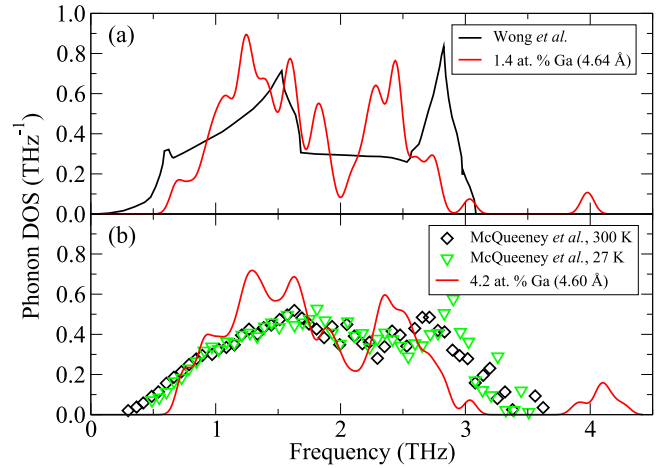


FIG. 2. Comparison of phonon densities of states (DOS) with experiment. The DOS calculated here employs the AFM structure in computational cells with 72 atoms; only phonons with commensurate wave vectors are shown, with the calculated frequencies convoluted with a Gaussian of width 0.05 THz. (a) The experimental data of Wong *et al.* [12] is calculated based on measurements on a  $\delta$ -Pu sample with 2 at. % Ga at room temperature. (b) The experimental data of McQueeney *et al.* [44] is measured on a  $\delta$ -Pu sample with 5 at. % Al at two temperatures; the sample at room temperature has a reported lattice constant of  $4.58 \text{ \AA}$ .

measured on  $\delta$ -Pu stabilized with 5 at. % Al [44] with the results from a calculation with 4.2 at. % Ga. The comparisons are not one-to-one: In addition to the approximate doping, the calculated DOS are based only on the phonons with wave vectors that are commensurate with the 72-atom computational cell. Given these approximations, the agreement with experiment is reasonable at low frequencies. The high-frequency peak in the calculated DOS is somewhat low, as expected from the behavior near the boundary of the first Brillouin zone (longitudinal [00 $\xi$ ] and [ $\xi\xi\xi$ ] branches) in Fig. 1. Absent from the experimental phonon DOS are the dopant-induced localized phonon modes seen in other experiments (see next section).

#### B. Single Ga substitution

Figure 3 compares the phonon density of states (DOS) of  $\delta$ -Pu to that of Pu-1.4 at. % Ga  $\delta$ -Pu (and higher concentrations). Most notably, the Ga substitution causes phonon modes to appear at frequencies well above those of  $\delta$ -Pu. The frequencies of these Ga substitution-induced modes agree well with the first moment for Ga, 3.94 THz, measured by Lynn *et al.* in Pu-3.6 at. % Ga  $\delta$ -Pu [45] and with the Ga-Pu bond Debye temperature of 3.92 THz, measured by Nelson *et al.* in Pu-1.9 at. % Ga  $\delta$ -Pu [17]. The calculated frequencies are a bit low compared to the Ga-Pu specific correlated-Debye temperature, 4.22 THz, measured by Allen *et al.* in Pu-3.3 at. % Ga  $\delta$ -Pu [46].

The appearance of phonon modes with frequencies that are well above those of  $\delta$ -Pu originates in the significantly lower mass of Ga. An instructive approximation for the effects of the substitution can be found by changing the mass of a single atom while retaining the force constants of the phonon

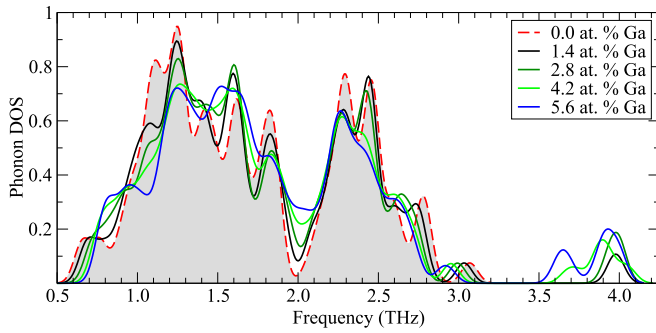


FIG. 3. Phonon densities of states calculated for  $\delta$ -Pu with and without Ga substitutions in a computational cell with 72 atoms at  $a_0 = 4.64 \text{ \AA}$ . The 213 ( $3 \times 72 - 3$ ) phonon frequencies are convoluted with a Gaussian of width 0.05 THz.

calculation for  $\delta$ -Pu. The results, shown in Fig. 4, reveal three phonon modes that, with decreasing mass, increase in both frequency and localization. Performing the DFT calculation with one Ga substitution shows that the changes to the ion positions and the force constants further increases the frequencies and especially the localization. Finally, the non-degeneracy of the localized modes in the approximation (due to the imposed asymmetric magnetic structure) is significantly reduced, especially the spatial asymmetry.

The frequencies and degree of localization for the complete set of phonon modes calculated for Pu-1.4 at. % Ga  $\delta$ -Pu appear in Fig. 5. The separation between Ga- and Pu-dominated modes is pronounced. The frequencies of the localized modes and their weight on the Ga atom change little for cell sizes larger than 36 atoms. The strong localization indicates they may well be described as a local Einstein mode considered as a possibility by Lynn *et al.* [45].

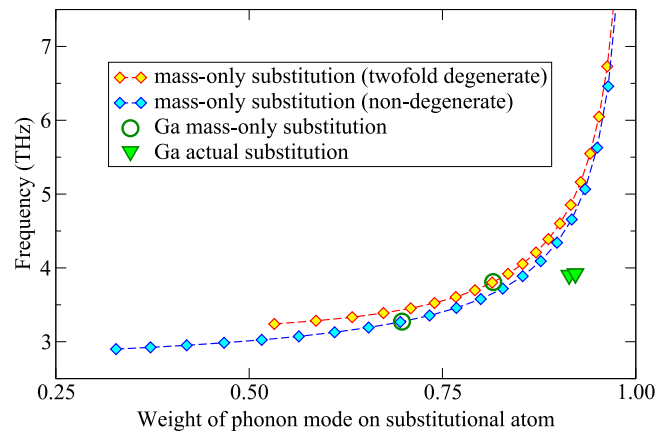


FIG. 4. Frequencies of localized phonon modes calculated for  $\delta$ -Pu with a single substitution in a computational cell with 64 atoms at  $a_0 = 4.64 \text{ \AA}$ , plotted versus the weight of the phonon modes on the substitutional atom. The data denoted as mass-only substitution are calculated by changing the mass of one atom (to values 110 a.u. and below, in steps of 5 a.u.) and using the force constants from the DFT calculation of the 64-atom  $\delta$ -Pu supercell. The data denoted as Ga actual substitution are calculated from the force constants of the 64-atom  $\delta$ -Pu supercell with one Ga substitution and relaxed atomic positions.

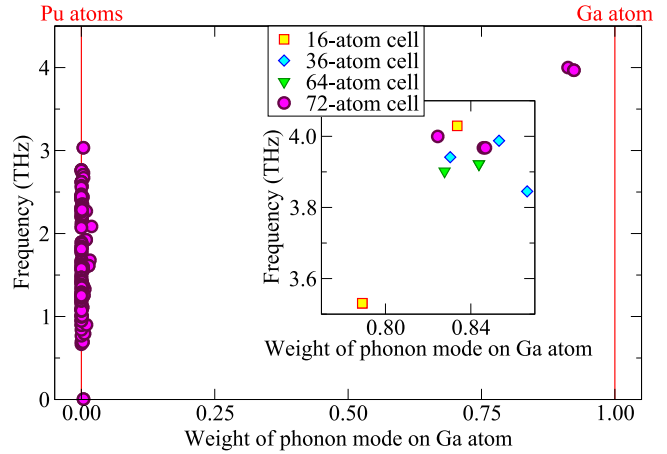


FIG. 5. Phonon mode frequencies calculated for  $\delta$ -Pu with a single Ga substitution in a computational cell with 72 atoms at  $a_0 = 4.64 \text{ \AA}$ , plotted versus the weight of the phonon mode on the Ga atom. Inset: Ga-dominated modes in computational cells with 16, 36, 64, and 72 atoms. Phonon modes with zero weight are completely described by a linear combination of the amplitudes of Pu atoms.

In the dilute limit, e.g., substituting one in 72 atoms, corresponding to 1.4 at. % Ga, changes to the Pu-dominated modes are subtle. Figure 6 reveals the subtle changes by plotting the weights of the bilinear projection [Eq. (2)]: the weights of the  $\delta$ -Pu phonon modes fall primarily on or near the diagonal. Small weights off the diagonal reflect a small degree of linear combining of the Pu-dominated modes as they adjust to form modes that no longer include the substituted Pu atom. The

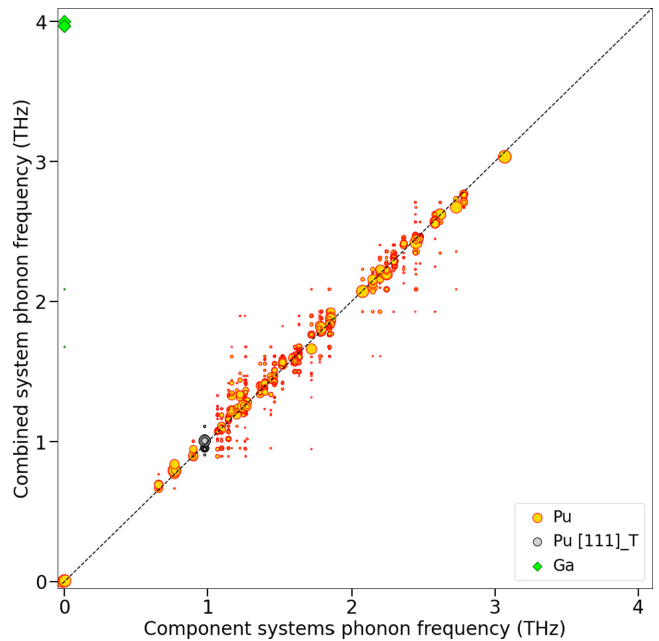


FIG. 6. Phonon mode tracing for  $\delta$ -Pu with one  $\text{Ga}_{\text{Pu}}$  substitution in computational cell with 72 atoms at  $a_0 = 4.64 \text{ \AA}$ . Orange circles represent  $\delta$ -Pu modes with black circles highlighting the  $T[111]$  modes; green diamonds represent Ga modes. The areas of the symbols are proportional to the weights as defined in Eq. (2); only weights larger than 0.01 are shown.



TABLE I. Energies and magnetic moments for two Ga substitutions in 72-atom fcc  $\delta$ -Pu cell at  $a_0 = 4.64 \text{ \AA}$ . The 72-atom cell is a  $3 \times 3 \times 2$ -conventional cell supercell, so the maximum distance from the first Ga substitution to the second Ga substitution in  $x$  and  $y$  is  $1.5 a_0$  and in  $z$  is  $1.0 a_0$ . The resulting magnetic moment is indicative of whether the two Ga atoms substitute Pu atoms with the same or opposite spins. The energy difference  $\Delta E$  is relative to that of two independent Ga substitutions, i.e.,  $\Delta E = [E(\text{Pu}_{70}\text{Ga}_2) - E(\text{Pu}_{72})] - 2[E(\text{Pu}_{71}\text{Ga}_1) - E(\text{Pu}_{72})]$ , and is evaluated with the finer ( $4 \times 4 \times 6$ ) k-point mesh. Some rows are left incomplete because the cost of phonon calculation outweighs the value of the results.

$\Delta x$	$\Delta y$ ( $a_0$ )	$\Delta z$	$d_{\text{Ga-Ga}}$ ( $\text{\AA}$ )	$\Delta E$ (meV)	mag ( $\mu_B$ )	$\omega_0$	$\omega_1$ (THz)	$\omega_2$
0	0.5	0.5	3.36	253	0	1.65	2.36	2.44
0.5	0.5	0	3.48	196	10.7	1.65	2.36	2.45
0	1	0	4.57	176	10.8			
0	0	1	4.64	257	11.2			
0.5	1	0.5	5.62	-9	0	1.66	2.37	2.45
0.5	0.5	1	5.64	-28	10.8	1.66	2.37	2.45
1	1	0	6.49	-18	10.9	1.67	2.38	2.45
0	1	1	6.53	-35	10.8	1.66	2.37	2.45
1.5	0.5	0	7.33	26	10.9			
0	1.5	0.5	7.34	32	0			
1	1	1	8.03	-37	10.8	1.66	2.38	2.46
1	1.5	0.5	8.67	-10	0	1.66	2.37	2.45
0.5	1.5	1	8.67	-11	10.7	1.66	2.37	2.45
1.5	1.5	0	9.84	11	10.5			
1.5	1.5	1	10.88	-25	10.8	1.66	2.38	2.46

frequencies remain very similar but show a slight stiffening at low frequencies and a slight softening at high frequencies. The change to the low-frequency modes provides a first hint that the stabilization might not be due to a thermodynamic mechanism: a thermodynamically more stable phase would be driven by a softening of the low-frequency modes that dominate the entropic term of the free energy.

Among the slightly stiffened phonon modes are phonon modes with wave vectors  $[\xi\xi\xi]T$ , in particular, the  $T[111]$  modes (highlighted). If these phonon modes initiate the pathway into the low-temperature phase, then an increase in their frequencies affects the initiation. The phonon frequencies describe only the local curvature in the delta phase and not the rest of the pathway. Hence increasing the curvature does not guarantee a higher energy barrier between the delta and the low-temperature phase. The increased curvature does, however, suggest that the pathway is likely less favorable.

### C. Multiple Ga substitutions

To address the effects of increased Ga concentration, first all unique arrangements of two Ga atoms (2.8 at. % Ga) in a 72-atom cell are considered. The energy cost of two Ga substitutions relative to twice that of a single substitutions, reported in Table I, shows a dramatic drop off beyond the second nearest-neighbor (NN) shell. Beyond this drop-off, the energy cost continues to vary, the most favored location being in rough agreement with all-electron DFT calculations [9].

Table I shows negligible dependence of the phonon moments on the Ga atoms' relative positions. (Consequently, the

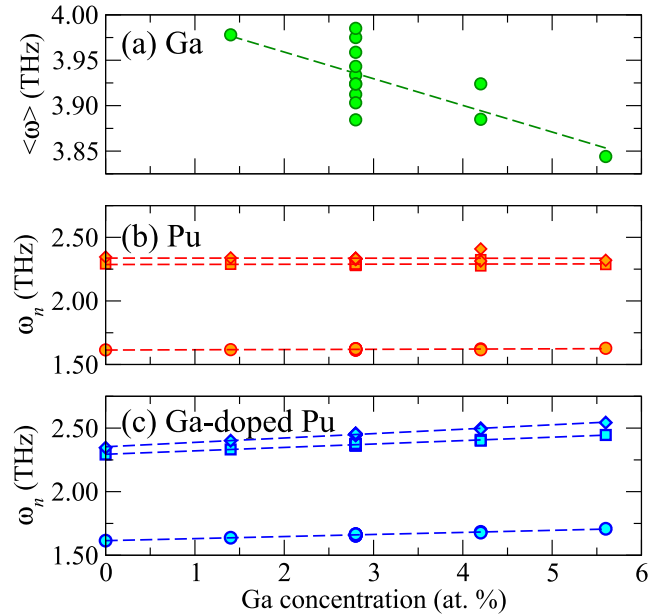


FIG. 7. Average frequency of Ga-dominated phonon modes (a), phonon moments for Pu-dominated phonon modes (b), and phonon moments for all phonon modes (c), calculated for Ga-doped  $\delta$ -Pu in computational cells with 72 atoms at  $a_0 = 4.64 \text{ \AA}$ . Data include one calculation at 1.4 at. % Ga, ten at 2.8 at. % Ga, two at 4.2 at. % Ga, and one at 5.6 at. % Ga.

phonon calculations were not performed for all configurations.) Small differences could be expected from allowing the volumes to relax. At the fixed volume, the preferred relative positions of the Ga substitutions appears not to involve thermal effects.

For larger concentrations, i.e., three and four substitutions, the calculations sample computational cells with well-separated Ga substitutions. These consist of two cells with three Ga atoms and one with four Ga atoms, with atoms arranged no closer than the fourth NN shell. The energy cost of these substitutions approximate the range of the double substitutions beyond the second Pu shell, with correspondingly defined  $\Delta E$  of 33 meV, 46 meV, and  $-47$  meV.

Figure 7(c) shows the phonon moments calculated for Ga-doped  $\delta$ -Pu increasing linearly with Ga concentration. The phonon moments calculated for only the Pu-dominated modes, shown in Fig. 7(b), exhibit no discernible change as the Ga concentration increases, indicating that the increase for Ga-doped  $\delta$ -Pu stems from the linear increase of the number of high-frequency, Ga-dominated modes. The average frequency of the Ga-dominated modes in Fig. 7(a) decreases slightly with increasing Ga concentration, signifying subtle interactions between the multiple Ga atoms.

The lack of discernible change in phonon moments of the Pu-dominated modes in Fig. 7(b) results from an averaging over phonon modes, some that stiffen and some that soften. The stiffening occurs mainly at lower frequencies, as seen in Fig. 8 (see Fig. 2 in the SM [24] for the complete frequency range). In particular, the eight transverse  $[111]$  modes at  $f = 0.98$  THz, which lose their degeneracy, become increasingly stiffer with increasing Ga concentration. Small weights of the

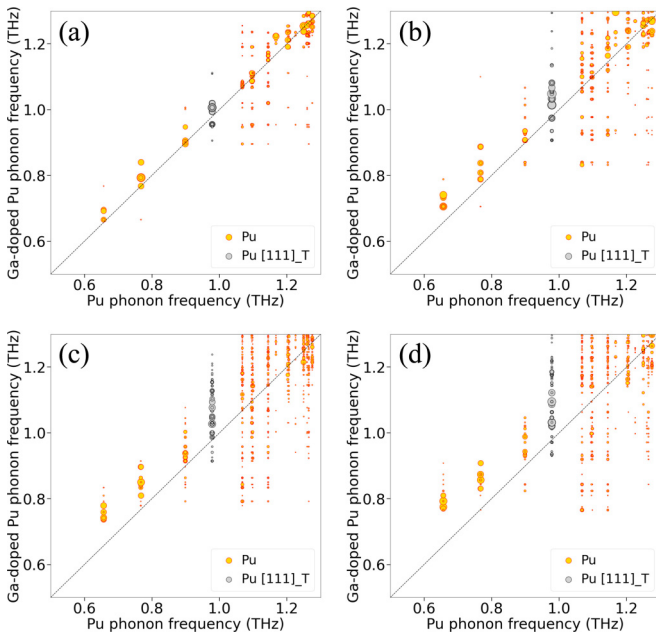


FIG. 8. Low-frequency excerpt of phonon frequency tracing for  $\delta$ -Pu with (a) one, (b) two, (c) three, and (d) four substitution Ga atoms in computational cell with 72 atoms at  $a_0 = 4.64$  Å. Orange circles represent the  $\delta$ -Pu modes with black circles highlighting the eight transverse [111] modes at  $f = 0.98$  THz (degenerate in undoped  $\delta$ -Pu). The areas of the symbols are proportional to the weights as defined in Eq. (2); only data with weight larger than 0.01 are shown.

$T[111]$  modes fall below the diagonal (i.e., below 0.98 THz) to couple with the mode originally at 0.90 THz, but these modes of Ga-doped  $\delta$ -Pu have minimal character related to the  $T[111]$  modes.

The results above by themselves suggest that a mechanism for Ga stabilization due to the phonons could involve impeding the proposed pathways. The low-frequency modes become stiffer with increased Ga concentration, thereby lessening the entropy that would favor thermodynamic stabilization. Furthermore, the zeroth phonon moment of both Ga-doped  $\delta$ -Pu and the Pu-dominated modes do not decrease with Ga concentration, and the zeroth phonon moment is the dominant quantity describing high-temperature entropy effects [25]. Among these stiffened modes are the  $[\xi\xi\xi]T$  modes suggested as pathways to the  $\alpha$ -Pu structure, indicating that Ga tends to block these pathways. The results supporting these arguments are all for a fixed volume, but allowing the volume to change should only add support: Ga doping contracts the volume, experimentally and theoretically [2,9], and smaller volume increases the forces, which leads to even stiffer phonons.

However, this last point, while generally true, does not completely hold for  $\delta$ -Pu. Figure 9(a) demonstrates an unusual softening of most lower-frequency modes in undoped  $\delta$ -Pu as the volume is compressed. The volume change is larger than that from Ga doping but serves to distinguish the differing behavior among phonon modes. This unusual behavior of phonon softening with compression likely relates to the unusual negative thermal expansion measured in

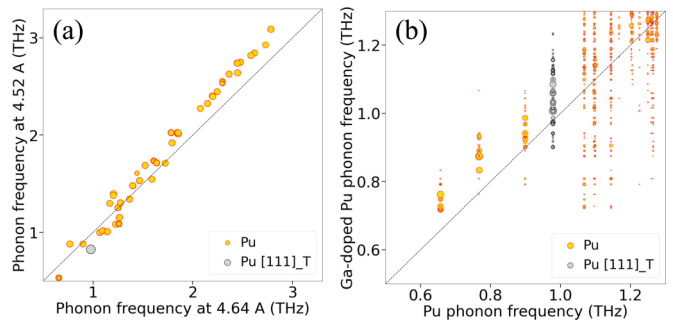


FIG. 9. Phonon frequency tracing from  $\delta$ -Pu at 4.64 Å (a) to  $\delta$ -Pu at  $a_0 = 4.52$  Å and (b) to Pu-4.2 at. % Ga  $\delta$ -Pu at  $a_0 = 4.60$  Å (the corresponding experimental lattice constant) in computational cells with 72 atoms. Orange circles represent the  $\delta$ -Pu modes with black circles highlighting the eight transverse [111] modes at  $f = 0.98$  THz (degenerate in undoped  $\delta$ -Pu). The areas of the symbols are proportional to the weights as defined in Eq. (2); only data with weights larger than 0.01 are shown.

$\delta$ -Pu [47]. To check how this softening due to the smaller volume compares with the stiffening due to Ga doping, the phonons are calculated for the 4.2 at. % Ga-doped system at the corresponding experimental lattice constant,  $a_0 = 4.60$  Å [2]. Figure 9(b) shows that the softening due to compression is more than offset by the Ga-doped stiffening (see Fig. 3 in the SM [24] for complete frequency range). This result is consistent with the suggestion that a mechanism for Ga stabilization due to the phonons could involve impeding the proposed pathways.

#### IV. DISCUSSION

DFT calculations on substitutional doping of  $\delta$ -Pu with Ga reveal two distinct types of phonon modes. The Ga atoms introduce high-frequency modes that are localized and separated in frequency from lower-frequency, Pu-dominated modes.

The Pu-dominated modes change their frequencies, and to some degree their character, with small concentrations of Ga doping. In particular, the low-frequency Pu-dominated modes stiffen, while the high-frequency Pu-dominated modes soften. Among the stiffened low-frequency Pu-dominated modes are those proposed to initiate a structural transformation into the  $\alpha$ -Pu structure. Increasing the Ga concentration enhances the stiffening. These results suggest that, as far as the phonons are concerned, the mechanism with which Ga doping stabilizes  $\delta$ -Pu is likely not by way of the free energy but rather by stiffening the initial slope of the structural transformation.

This suggestion comes with caveats. It does not consider how Ga changes the low-frequency modes of the other phases: if those were stiffened to an even larger degree, thermodynamic stabilization would play a role. It does not consider the effects of self-irradiation, which leaves Pu with significant damage; chemical analysis of Ga-doped Pu shows many impurities [48]. These defects can partially be annealed out [49] but any sample history leaves lattice imperfections that can affect the structural phase transformation. DFT calculations

predict interactions between Ga and such lattice imperfections [18].

Additional support for a pathway-impeding mechanism comes from considering volume effects. Compressing Ga-doped  $\delta$ -Pu can transform the crystal into the Ga-doped alpha phase, but only for small amounts of Ga: larger Ga concentration inhibits the transformation with compression [48]. The present calculations show that Ga doping and compression have opposing effects on the phonon frequencies. If the transformation is initiated by a softening with compression of, e.g., the  $T[111]$  phonon mode, aided by lattice imperfections, does Ga doping still stiffen the mode more than

compression softens it? Research aimed at just this issue is underway.

#### ACKNOWLEDGMENTS

This work was supported by the U.S. DOE through Contract No. 89233218CNA000001 via the LANL Laboratory Directed Research and Development Program. The author thanks E. Bauer, S. Crockett, A. Fredenburg, F. Freibert, S. Hernandez, J. Mitchell, and R. Tutchton for helpful and encouraging discussions and S. Halverson for generous computational support.

- 
- [1] L. Lindsay, A. Katre, A. Cepellotti, and N. Mingo, *J. Appl. Phys.* **126**, 050902 (2019).
- [2] F. H. Ellinger, C. C. Land, and V. O. Struebing, *J. Nucl. Mater.* **12**, 226 (1964).
- [3] S. S. Hecker and L. F. Timofeeva, *Los Alamos Sci.* 244 (2000).
- [4] S. Hecker, D. Harbur, and T. Zocco, *Prog. Mater. Sci.* **49**, 429 (2004), a Festschrift in Honor of T. B. Massalski.
- [5] A. Landa and P. Söderlind, *J. Alloys Compd.* **354**, 99 (2003).
- [6] B. Sadigh and W. G. Wolfer, *Phys. Rev. B, Condens. Matter* **72**, 205122 (2005).
- [7] G. Robert, A. Pasturel, and B. Siberchicot, *Phys. Rev. B* **68**, 075109 (2003).
- [8] K. T. Moore, P. Söderlind, A. J. Schwartz, and D. E. Laughlin, *Phys. Rev. Lett.* **96**, 206402 (2006).
- [9] S. C. Hernandez, D. S. Schwartz, C. D. Taylor, and A. K. Ray, *J. Phys.: Condens. Matter* **26**, 235502 (2014).
- [10] S. C. Hernandez and F. J. Freibert, *Appl. Sci.* **10**, 7628 (2020).
- [11] P. Söderlind, A. Landa, J. E. Klepeis, Y. Suzuki, and A. Migliori, *Phys. Rev. B* **81**, 224110 (2010).
- [12] J. Wong, M. Krisch, D. L. Farber, F. Occelli, R. Xu, T.-C. Chiang, D. Clatterbuck, A. J. Schwartz, M. Wall, and C. Boro, *Phys. Rev. B* **72**, 064115 (2005).
- [13] R. Xu, J. Wong, P. Zschack, H. Hong, and T.-C. Chiang, *Europhys. Lett.* **82**, 26001 (2008).
- [14] B. Dorado, F. Bottin, and J. Bouchet, *Phys. Rev. B* **95**, 104303 (2017).
- [15] T. Lookman, A. Saxena, and R. C. Albers, *Phys. Rev. Lett.* **100**, 145504 (2008).
- [16] R. Gröger, T. Lookman, and A. Saxena, *Philos. Mag.* **89**, 1779 (2009).
- [17] E. J. Nelson, K. J. M. Blobaum, M. A. Wall, P. G. Allen, A. J. Schwartz, and C. H. Booth, *Phys. Rev. B* **67**, 224206 (2003).
- [18] S. Hernandez, F. Freibert, and J. Wills, *Scr. Mater.* **134**, 57 (2017).
- [19] G. Kresse and J. Furthmüller, *Phys. Rev. B* **54**, 11169 (1996).
- [20] G. Kresse and D. Joubert, *Phys. Rev. B* **59**, 1758 (1999).
- [21] P. E. Blöchl, *Phys. Rev. B* **50**, 17953 (1994).
- [22] J. P. Perdew, K. Burke, and M. Ernzerhof, *Phys. Rev. Lett.* **77**, 3865 (1996).
- [23] M. Methfessel and A. T. Paxton, *Phys. Rev. B* **40**, 3616 (1989).
- [24] See Supplemental Material at <http://link.aps.org/supplemental/10.1103/PhysRevB.105.184107> for additional phonon frequency tracings.
- [25] D. C. Wallace, *Statistical Physics of Crystals and Liquids* (World Scientific, Singapore, 2002).
- [26] T. Sjöstrom, S. Crockett, and S. Rudin, *Phys. Rev. B* **94**, 144101 (2016).
- [27] D. A. Rehn, C. W. Greeff, D. G. Sheppard, and S. Crockett, *Using Density Functional Theory to Construct Multiphase Equations of State: Tin as an Example*, Tech. Rep. No. LA-UR-20-29170 (Los Alamos National Laboratory, Los Alamos, NM, 2020).
- [28] H. L. Skriver, O. K. Andersen, and B. Johansson, *Phys. Rev. Lett.* **41**, 42 (1978).
- [29] P. Soderlind, *Eur. Phys. Lett.* **55**, 525 (2001).
- [30] G. Robert, A. Pasturel, and B. Siberchicot, *J. Phys.: Condens. Matter* **15**, 8377 (2003).
- [31] P. Soderlind and B. Sadigh, *Phys. Rev. Lett.* **92**, 185702 (2004).
- [32] P. Söderlind, A. Landa, and B. Sadigh, *Adv. Phys.* **68**, 1 (2019).
- [33] J. C. Lashley, A. Lawson, R. J. McQueeney, and G. H. Lander, *Phys. Rev. B* **72**, 054416 (2005).
- [34] M. Janoschek, P. Das, B. Chakrabarti, D. L. Abernathy, M. D. Lumsden, J. M. Lawrence, J. D. Thompson, G. H. Lander, J. N. Mitchell, S. Richmond, M. Ramos, F. Trouw, J.-X. Zhu, K. Haule, G. Kotliar, and E. D. Bauer, *Sci. Adv.* **1**, e1500188 (2015).
- [35] P. Soderlind, A. Landa, B. Sadigh, L. Vitos, and A. Ruban, *Phys. Rev. B* **70**, 144103 (2004).
- [36] P. Söderlind, F. Zhou, A. Landa, and J. E. Klepeis, *Sci. Rep.* **5**, 15958 (2015).
- [37] P. Söderlind and A. Landa, *J. Nucl. Mater.* **448**, 310 (2014).
- [38] V. Arkhipov, F. Kassan-Ogly, A. Korolev, S. Verkhovskii, Y. Zuev, and I. Svyatov, *J. Nucl. Mater.* **385**, 42 (2009), plutonium Futures - The Science 2008.
- [39] B. Dorado, J. Bieder, and M. Torrent, *J. Phys.: Condens. Matter* **29**, 245402 (2017).
- [40] G. Kresse, J. Furthmüller, and J. Hafner, *Europhys. Lett.* **32**, 729 (1995).
- [41] D. Alfè, G. D. Price, and M. J. Gillan, *Phys. Rev. B* **64**, 045123 (2001).
- [42] D. Alfè, *Comput. Phys. Commun.* **180**, 2622 (2009), 40 Years of CPC: A celebratory issue focused on quality software for high performance, grid and novel computing architectures.
- [43] X. Dai, S. Y. Savrasov, G. Kotliar, A. Migliori, H. Ledbetter, and E. Abrahams, *Science* **300**, 953 (2003).

- [44] R. J. McQueeney, A. C. Lawson, A. Migliori, T. M. Kelley, B. Fultz, M. Ramos, B. Martínez, J. C. Lashley, and S. C. Vogel, *Phys. Rev. Lett.* **92**, 146401 (2004).
- [45] J. E. Lynn, G. H. Kwei, W. J. Trela, V. W. Yuan, B. Cort, R. J. Martínez, and F. A. Vigil, *Phys. Rev. B* **58**, 11408 (1998).
- [46] P. G. Allen, A. L. Henderson, E. R. Sylwester, P. E. A. Turchi, T. H. Shen, G. F. Gallegos, and C. H. Booth, *Phys. Rev. B* **65**, 214107 (2002).
- [47] A. C. Lawson, J. A. Roberts, B. Martínez, M. Ramos, G. Kotliar, F. W. Trouw, M. R. Fitzsimmons, M. P. Hehlen, J. C. Lashley, H. Ledbetter, R. J. McQueeney, and A. Migliori, *Philos. Mag.* **86**, 2713 (2006).
- [48] S. Ennaceur, *Thermochim. Acta* **601**, 17 (2015).
- [49] C. H. Booth, Y. Jiang, S. A. Medling, D. L. Wang, A. L. Costello, D. S. Schwartz, J. N. Mitchell, P. H. Tobash, E. D. Bauer, S. K. McCall, M. A. Wall, and P. G. Allen, *J. Appl. Phys.* **113**, 093502 (2013).